Electronic Supplementary Information (ESI) for:

Excitation Ratiometric Chloride Sensing in a Standalone Yellow Fluorescent Protein is Powered by the Interplay between Proton Transfer and Conformational Reorganization

Cheng Chen,[†] Jasmine N. Tutol,[‡] Longteng Tang,[†] Liangdong Zhu,[†] Whitney S. Y. Ong,[‡] Sheel C. Dodani,*[,‡] and Chong Fang*[,†]

[†]Department of Chemistry, Oregon State University, 153 Gilbert Hall, Corvallis, Oregon 97331, United States

[‡]Department of Chemistry and Biochemistry, The University of Texas at Dallas, Richardson, Texas 75080, United States

*To whom correspondence should be addressed.

E-mail: Chong.Fang@oregonstate.edu or Sheel.Dodani@utdallas.edu.

Table of Contents

1. Experimental and Computational Methods

1.1. Protein expression and sample preparation

The reagents, instruments, and plasmid encoding the wild-type yellow fluorescent protein from *Phialidium sp.* (phiYFP, UniProt ID: Q6RYS7) used in this study were previously described.[1] The large-scale expression and purification methods of phiYFP were adapted with the following modifications. Briefly, single colonies of *E. cloni* EXPRESS BL21(DE3) Competent Cells were transformed with a freshly prepared plasmid and inoculated into 50 mL of 2xYT media containing 50 μg/mL kanamycin sulfate in 250 mL baffled flasks. After incubation at 37 °C with shaking at 230 rpm for 18 h, 24 mL of the overnight culture was inoculated into 1.2 L of 2xYT media containing 50 μg/mL kanamycin sulfate in 4 L baffled flasks and incubated at 37 °C with shaking at 150 rpm. When the OD_{600} reached ~0.6−0.8, protein expression was induced by adding 1.2 mL of 1 M isopropyl-β-D-thiogalactoside (IPTG) in water to a final concentration of 1 mM IPTG. After 24 h, the cells were harvested by centrifugation at 2,500*g* for 20 min at 4 °C, resuspended in 100 mL of the resuspension buffer containing 20 mM Tris buffer at pH=7.5, 200 mM sodium chloride, 5 mM magnesium chloride, 30 μg/mL deoxyribonuclease I, and one protease inhibitor tablet, and stored at −20 °C.

On the day of purification, the cells were thawed at room temperature for 30 min and diluted with an additional 50 mL of the resuspension buffer, followed by lysis using sonication at 50% amplitude, 20 s pulse on, and 40 s pulse off for 20 min. The cell debris was removed using ultracentrifugation at 18,000*g* for 40 min at 4 °C and, the supernatant was further clarified using ultracentrifugation at 37,000*g* for 20 min at 4 °C. For each protein batch, 50 mL of the resulting supernatant was loaded at a flow rate of 2 mL/min onto pre-equilibrated 5-mL nickel nitrilotriacetic acid (Ni-NTA) column using a flash protein liquid chromatography system. The column was then

washed with 7 column volumes (CV) of 20 mM Tris running buffer at pH=7.5 containing 200 mM sodium chloride and 30 mM imidazole at a flow rate of 5 mL/min. Then, the protein was eluted with a mixture 50% of the running buffer and 20 mM Tris elution buffer at pH=7.5 containing 200 mM sodium chloride, and 500 mM imidazole for 3–5 CV and 100% of the elution buffer for 10 CV. This process was repeated until all of the clarified lysate was purified. For each batch, all of the fractions with an absorbance at 525 nm were combined together and then buffer-exchanged three times with 50 mM 2-(*N*-morpholino)ethanesulfonic acid buffer (MES) at pH=5.5 containing 400 mM sodium chloride or 400 mM sodium nitrate, or with 50 mM sodium citrate buffer at pH=4.5 (apo phiYFP, chromophore pK_a=4.9), 400 mM sodium chloride (with the anion binding, chromophore pK_a=5.4)[1] or 400 mM sodium nitrate using a centrifugal filter with a 10 kDa molecular weight cut-off. After the buffer exchange, protein samples were concentrated to ~0.2−0.8 mM stored at 4 °C until further use. For each sample, the total protein concentration was determined using the Pierce Coomassie (Bradford) Protein Assay Kit according to the manufacturer's instructions. Two batches of proteins (technical replicates) were prepared and studied, and the representative spectral data in pH=5.5 buffer solution were shown and analyzed in this work.

1.2. Chromophore pK_a determination

The chromophore pK_a of phiYFP was determined in the absence and presence of 400 mM sodium chloride or 400 mM sodium nitrate. For these measurements, two batches of protein were purified as described above but buffer exchanged into 20 mM sodium phosphate buffer containing 200 mM sodium gluconate at pH=7. For each batch, the protein was diluted to a final concentration of 40 μM in 50 mM sodium acetate buffer from pH=4–5.5 or 50 mM sodium phosphate buffer from

pH=5.5–9, followed by further dilution to 5 μM in the corresponding buffers containing 0 mM or 457 mM of sodium chloride or 457 mM sodium nitrate. Two aliquots of each sample (200 μL/well) were transferred to a 96-well microtiter plate. For each well, the absorbance spectrum was collected from 300–650 nm with a 5 nm step size on a Tecan Spark plate reader. To determine the chromophore pK_a, the absorbance values at 400 nm and 525 nm versus the pH were fitted to the Henderson–Hasselbalch equation in KaleidaGraph v4.5 (see **Figure S3** below). The reported pK_a values of phiYFP in **Table 1** (main text) were averaged over four replicates for the spectral data at both 400 nm and 525 nm.

1.3. Spectroscopic measurements and target analysis

The femtosecond transient absorption (fs-TA) spectra for all the phiYFP samples were collected using a home-built optical setup[2,3] based on a mode-locked Ti:sapphire oscillator and a laser regenerative amplifier (Legend Elite-USP-1K-HE, Coherent, Inc.) that provides an 800 nm fundamental pulse (FDP) with 35 fs duration and 1 kHz repetition rate. The 400 nm pump pulse was generated from the second harmonic of the FDP and then compressed by a prism pair (06SB10, transmission range of 185 nm to 2.1 μm, Newport, Inc.). The probe pulse (supercontinuum white light) was generated by focusing a portion of the FDP onto a 2-mm-pathlength quartz cuvette filled with deionized water and then compressed by a chirp mirror pair (DCM-12, 400−700 nm, Laser Quantum, Inc.). The cross-correlation time for these measurements was measured to be 70−80 fs.[3,4] The sample was housed in a 1-mm-pathlength quartz cuvette (48-Q-1, Starna Cells) and flowed through soft tubing, pumped by a mini electric motor (Gikfun 12V DC peristaltic pump). The steady-state absorption spectra were collected with a Thermo Scientific Evolution 201 UV/Visible spectrophotometer with sample solution filled in a 1-mm-pathlength quartz cuvette (1-

Q-1, Starna Cells). The steady-state fluorescence spectra were collected with a Shimadzu RF-6000 spectrofluorophotometer with sample solution housed in a four-sided, 10-mm-pathlength quartz cuvette. All the experiments were performed at room temperature (22 °C) and 1 atm.

To delineate the underlying species from the overlapped electronic bands in our fs-TA data (e.g., see **Figure 3** in main text and **Figures S9** below), we performed the target analysis using the software Glotaran[5] and set up the kinetic model by the transfer matrix K:[6,7]

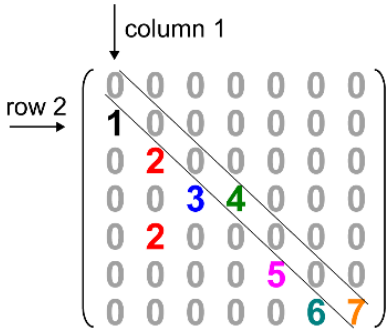

The spectral transitions are represented by the non-zero off-diagonal elements (color-coded as **Figure 5a** in main text) where the column and row indices denote the preceding and succeeding states/species, respectively. For example, the element K_{21} labeled by number "**1**" represents the transition from state 1 to state 2, and so on. Notably, two identical numbers "**2**" in column 2 and rows 3 and 5 indicate the ultrafast branching of reaction pathways (i.e., state 2 to state 3, and state 2 to state 5 as reflected by the kinetic scheme in **Figure 5a**). The non-zero diagonal elements denote the self-decay of the corresponding states (i.e., states 4 and 7).

1.4. Computational methods

To calculate the electronic energy gap of the phiYFP chromophore and estimate the effect of π-π stacking interaction, the starting structure that consists of the chromophore core (with the same structure as *p*-HBDI),[3,8] an adjacent water molecule, and the side chain of Y203 was directly taken

from the crystal structure of phiYFPv (PDB ID: 4HE4), a phiYFP mutant with improved folding and ten amino-acid mutations from its progenitor wild-type phiYFP outside the chromophore area (mostly positioned on the protein surface exposed to solvent).[9] We consider that these moieties in the immediate vicinity of the chromophore are crucial in determining the electronic transition gap of the biosensor based on YFP, while the specific halogen-binding site differs in location from that in E^2GFP (also with T203Y, but based on GFP) as indicated by the crystallographic analyses.[10,11] Focusing on the main structural factor, the coordinates of two "stacked" benzene rings on the chromophore and Y203 (in the antiparallel configuration, $d \approx 3.6$ Å between the nearly perfect antiparallel phenolic rings of the chromophore Y66 and Y203 in PhiYFPv)[9] were fixed during our calculations, hence their π-π interaction was maintained during the geometrical optimization. During such calculations, without fixing the nuclear coordinates, the benzene ring of Y203 would flip away from the chromophore due to the steric/electrostatic repulsion, leading to a very unreasonable structure. Therefore, we tested fixing different atoms of the chromophore (Y66) and Y203 during our calculations and found that fixing all the atoms on the benzene rings yield the most reasonable structure and results after geometrical optimization of all the remaining structural units. To model the neutral chromophore (**Figure S12**), a proton was added to the Y66 phenolate group. The structures were optimized consecutively with 3-21G, 6-31G, 6-31G(d, p), and 6-31G+(d, p) basis sets *in vacuo* at the B3LYP level of density functional theory (DFT) using the Gaussian 16 program.[12]

After optimization, in order to model the anionic species in an unrelaxed protein environment (I*) as a result of excited-state proton transfer (ESPT, see main text),[1,13,14] we twisted the Y203 side-chain benzene ring along the H−C−C angle on the methyl group connected to the benzene ring by 20°, 40°, and 60° to explore the effect of Y203 stacking configuration on the electronic

transition gap of the adjacent deprotonated chromophore (**Figure S14**). The twisted structures were then optimized with 6-31G+(d,p) basis sets, note that the two adjacent benzene rings remain fixed (Cartesian coordinates were frozen to maintain the specific stacking configuration) during optimization hence the final optimized structure has the same H−C−C angle as the common methyl group configuration. The S_1–S_0 energy gaps based on the vertical excitation at the ground-state optimized structures were calculated with the time-dependent (TD)-DFT method and B3LYP functional to be consistent. The calculation results are plotted and summarized in **Figure S12** (for the protonated chromophore with and without Y203) and **Figure S14** (for the deprotonated chromophore with and without Y203, plus three representative twisting angles that diminish the π-π stacking interactions) below, and it is clear that calculations for both A and B chains in the phiYFPv crystal structure[9] yielded consistent results. In essence, these readily available and affordable DFT- and TD-DFT-based quantum calculations *in vacuo*, though less advanced or comprehensive than a full-scale high-level QM/MM simulation on the entire protein with a photoexcited chromophore and dynamic ion binding events, still provide a robust pattern of the S_1–S_0 energy gap by *including* and *twisting* the important Y203 residue in close proximity to the protein chromophore. Such a pattern lends solid support to the experimentally observed I_1* and I_2* species without and with significant π-π stacking interactions, respectively (see main text).

2. Supplementary Figures

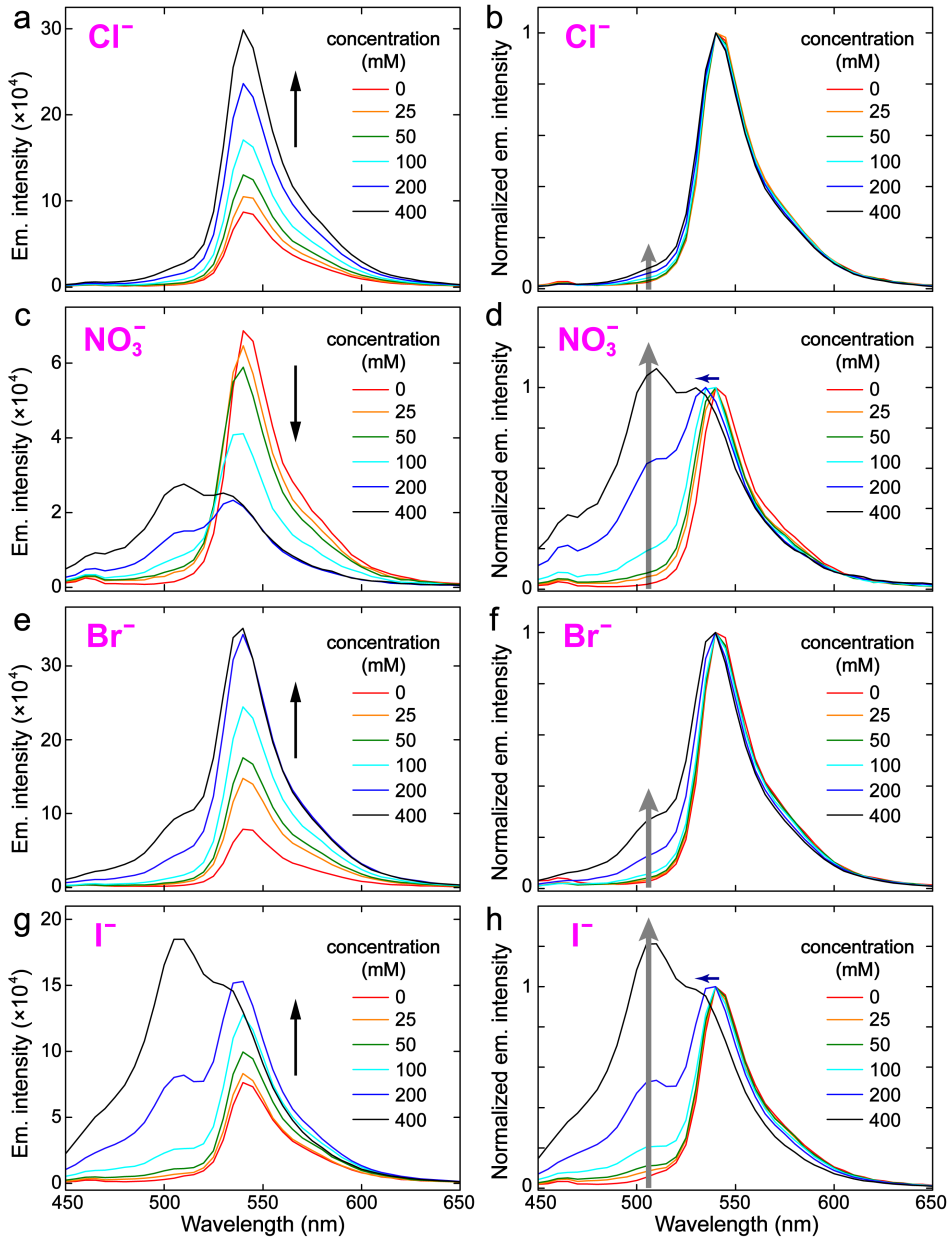

Figure S1. Fluorescence spectra of phiYFP in 50 mM MES buffer at pH=5.5 with various concentrations of different anions, particularly 0–400 mM (a) Cl^-, (c) NO_3^-, (e) Br^-, (g) I^-. The protein concentration was 5 μM. Excitation was provided at 400 nm. The black arrows denote increasing anion concentrations (the color-coded data used from our previous report).[1] The normalized fluorescence spectra (at the I_2* peak around 540 nm, see **Table 1**) are shown in (b),

(d), (f), and (h) for Cl^-, NO_3^-, Br^-, and I^-, respectively, with gray arrows highlighting the relative increase of I_1* peak around 505 nm. The notable blueshift of the I_2* peak for phiYFP with an increasing concentration of NO_3^- and I^- (with relatively strong binding, see main text) is shown by the horizontal blue arrows in panels (d) and (h).

Upon 400 nm excitation of the neutral chromophore of phiYFP in buffer solution,[1] while the I_2* emission intensity manifests the opposite trend, the common increase of the I_1* emission intensity with addition of Cl^-/NO_3^- (**Figure S1a,c**) is due to the increased pK_a that leads to more A* excitation and hence more ESPT population (see main text, and note the determination of pK_a values from absorption spectra in Section 1.2 above). Moreover, the relative increase of I_1* to I_2* emission intensity with addition of Cl^-/NO_3^- (**Figure S1b,d**) suggests that the binding of Cl^- and NO_3^- both inhibits the I_1*→I_2* conversion but to different extents (see **Figure 6**). The additional spectral data in the presence of Br^- and I^- (**Figure S1f,h**) further confirm the mechanism as their binding affinities to phiYFP are in between the Cl^- and NO_3^- cases.[1] Note that we focus on the two extreme ends (400 mM chloride and nitrate, see main text) in terms of anion binding affinities in this work, while the ubiquitous presence of chloride in cellular environments contrasts with nitrate that is unlikely to exist in mammalian cells at such a high concentration, thus allowing us to delineate a unified phiYFP potential energy surface (**Figure 6** in main text) that enables its dramatically different excitation-ratiometric fluorescence response to chloride (less so for the other halides) from other oxyanions like nitrate (see **Figure S1** above).

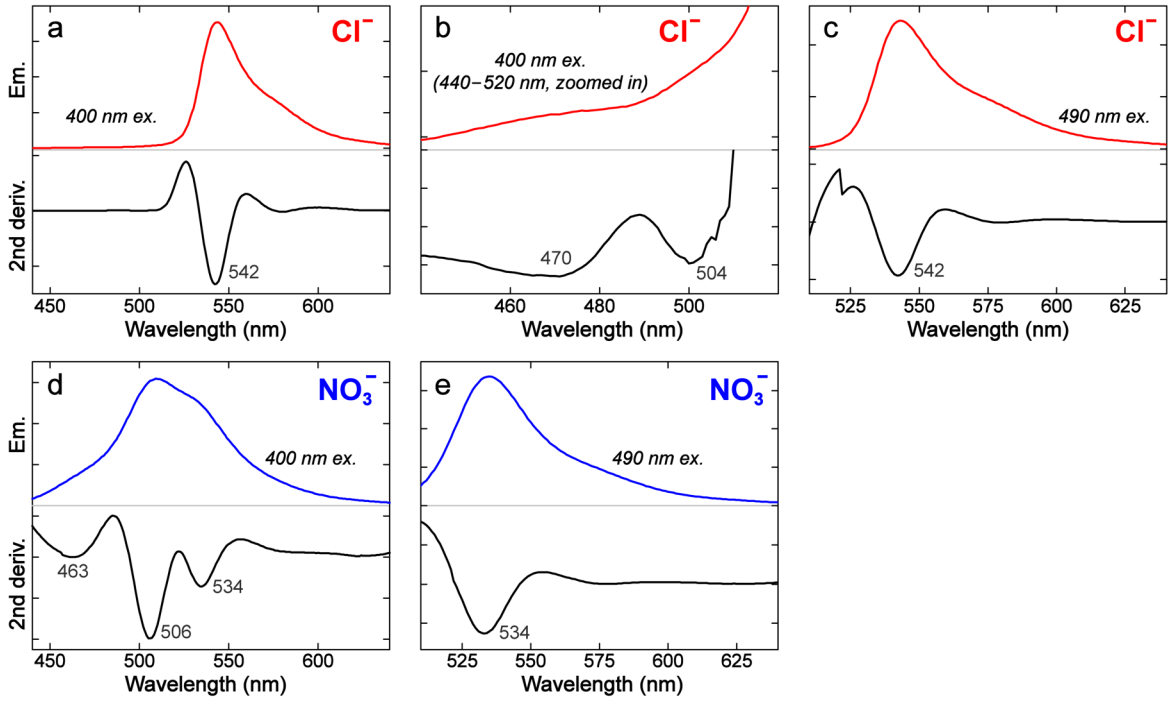

Figure S2. Second-derivative analysis of fluorescence spectra for phiYFP in pH=5.5 buffer. The steady-state emission spectra of phiYFP with 400 mM (a) Cl^- and (d) NO_3^- in 50 mM MES buffer solution upon 400 nm excitation are shown with the enlarged short-wavelength region from 440–520 nm in (b) for the Cl^--bound case. The corresponding emission spectra upon 490 nm excitation are displayed in (c) and (e). The peak locations are denoted by the second-derivative traces (black) and tabulated in **Table 1** (see main text).

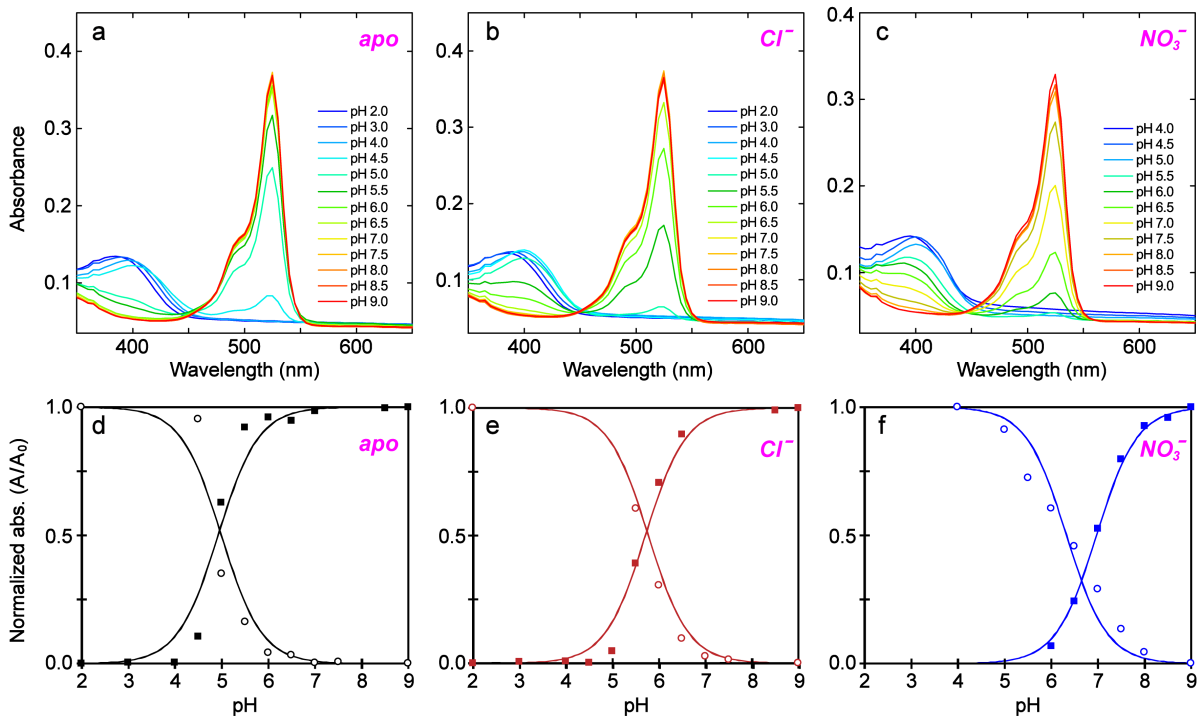

Figure S3. Determination of pK_a from pH-dependent absorption spectra of phiYFP in buffer solution. Steady-state electronic absorption spectra (upper panels) and pK_a titration curves (bottom panels) in the absence (apo, panels *a* and *d*) and presence of 400 mM Cl^- (panels *b* and *e*) and NO_3^- (panels *c* and *f*). The pK_a values listed in **Table 1** in main text were obtained by averaging the two pK_a values from the titration curves (panels *d*, *e*, and *f*) for the neutral (400 nm, hollow circles) and anionic (525 nm, solid squares) forms of the phiYFP chromophore (see Section 1.2 above). The fits to the Henderson–Hasselbalch equation in KaleidaGraph v4.5 are shown as solid curves overlaid with spectral data points in black, red, and blue in panels (d), (e), and (f), respectively.

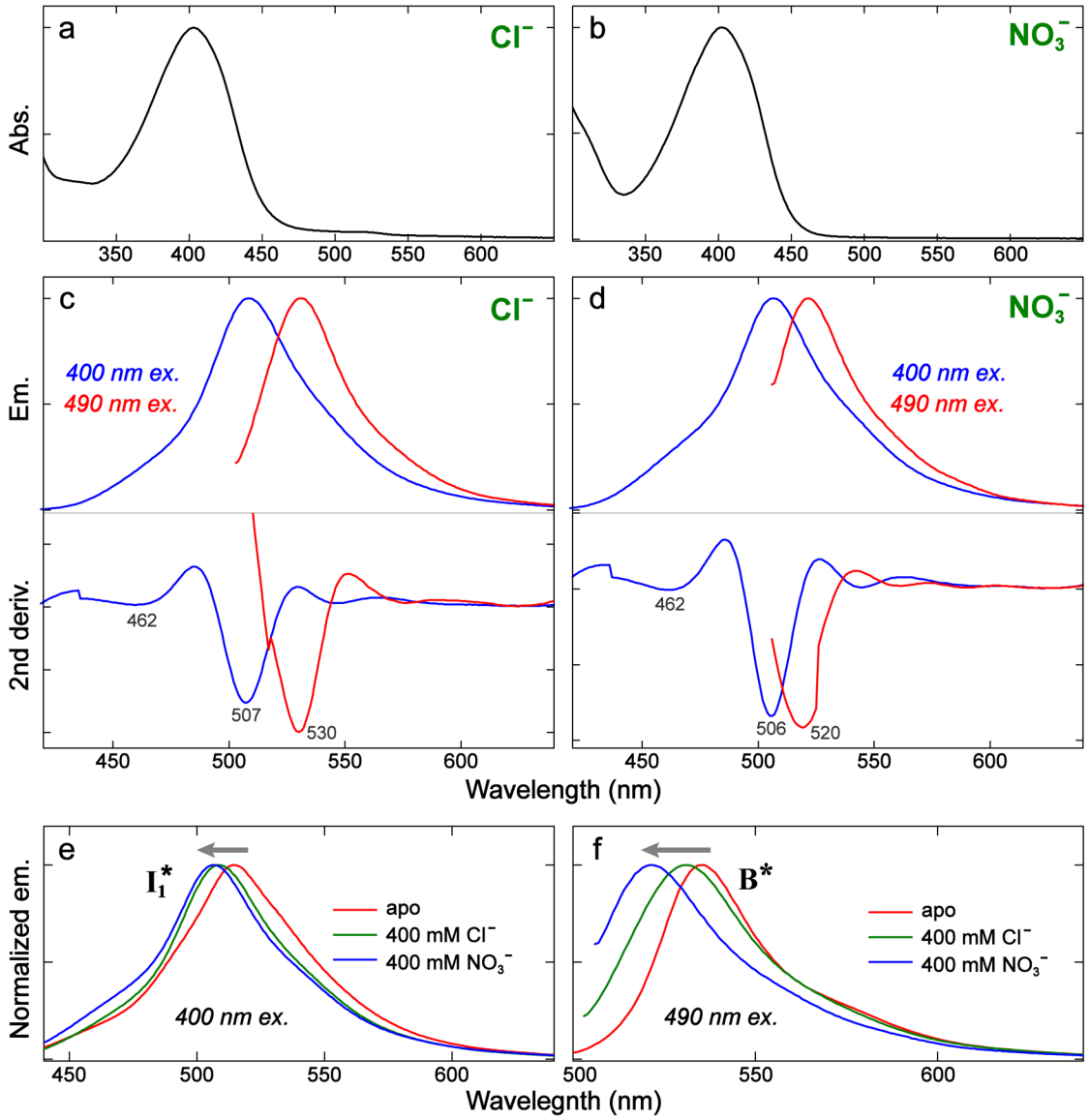

Figure S4. Excitation- and anion-dependent fluorescence spectra of phiYFP in 50 mM sodium citrate buffer at pH=4.5. The steady-state absorption (upper panels) and emission (middle panels) spectra of phiYFP with 400 mM (a, c) Cl^- and (b, d) NO_3^- upon 400 nm (blue) or 490 nm (red) excitation are shown. The second-derivative traces of the emission spectra are displayed below with the A* and I_1* (blue) and I_2* (red) peak positions labeled. The notable blueshift of (e) I_1* and (f) B* emission peaks from phiYFP without anions (apo structure, red), with 400 mM Cl^- (green) to that with 400 mM NO_3^- (blue) is denoted by the horizontal gray arrow.

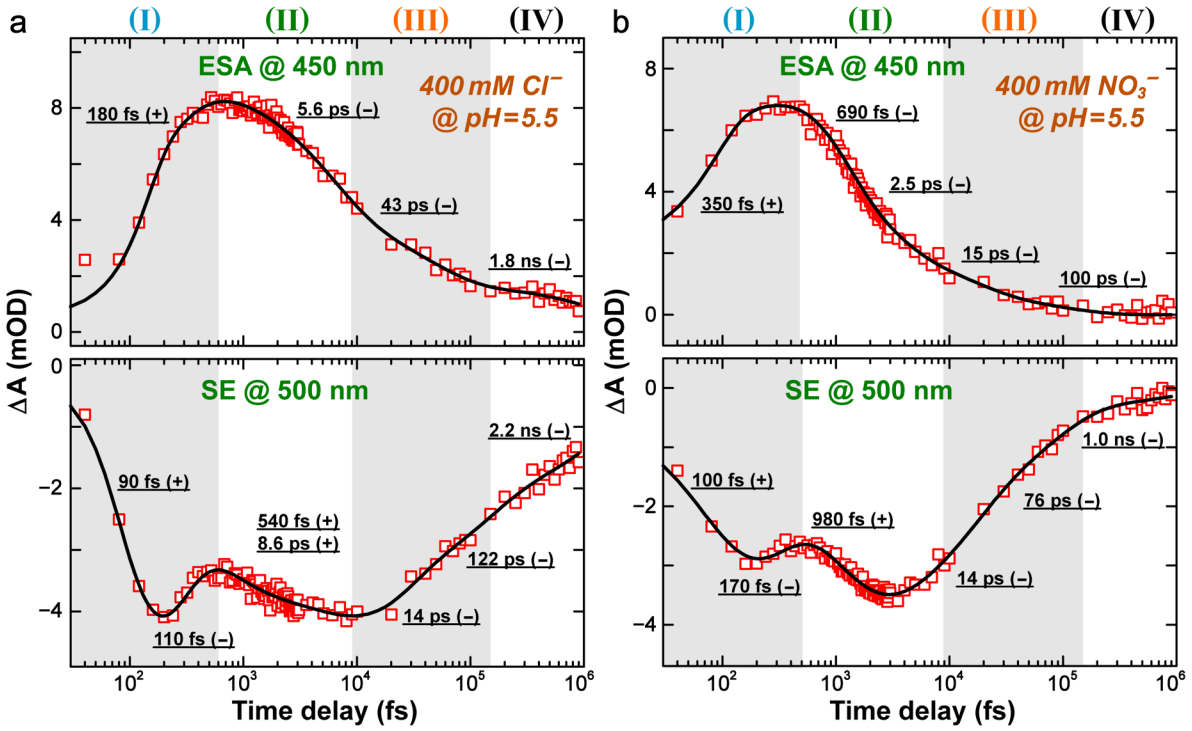

Figure S5. Probe-wavelength-dependent fs-TA dynamics of phiYFP in 50 mM MES buffer at pH=5.5 with anions: 400 mM (a) Cl^- and (b) NO_3^-. The time-resolved data points (red squares) from raw experimental spectra at 450 nm ESA band and 500 nm SE band (see Figure 3 in main text and Figure S9 below) are overlaid with the least-squares fits (solid black traces). The retrieved time constants are listed by their dynamic processes with the (+) and (–) signs denoting the signal intensity rise and decay, respectively (see tabulated values in **Table S2**). The distinctive four stages, (I) to (IV), are highlighted by alternating gray and white shades which have their characteristic time constants (see main text). ESA: excited-state absorption, SE: stimulated emission.

Together with **Figures 3–5** (main text), the observed I_2* SE peak at ~530 nm is on the blue side of the steady-state fluorescence peak of phiYFP in the presence of 400 mM Cl^- (542 nm) and NO_3^- (534 nm). This result indicates that further structural relaxation occurs on the ns and longer timescales (beyond our detection time window) toward the final emissive state,[15] while the weaker Cl^- binding leads to a larger redshift (~12 nm) than that with stronger NO_3^- binding (~4 nm).

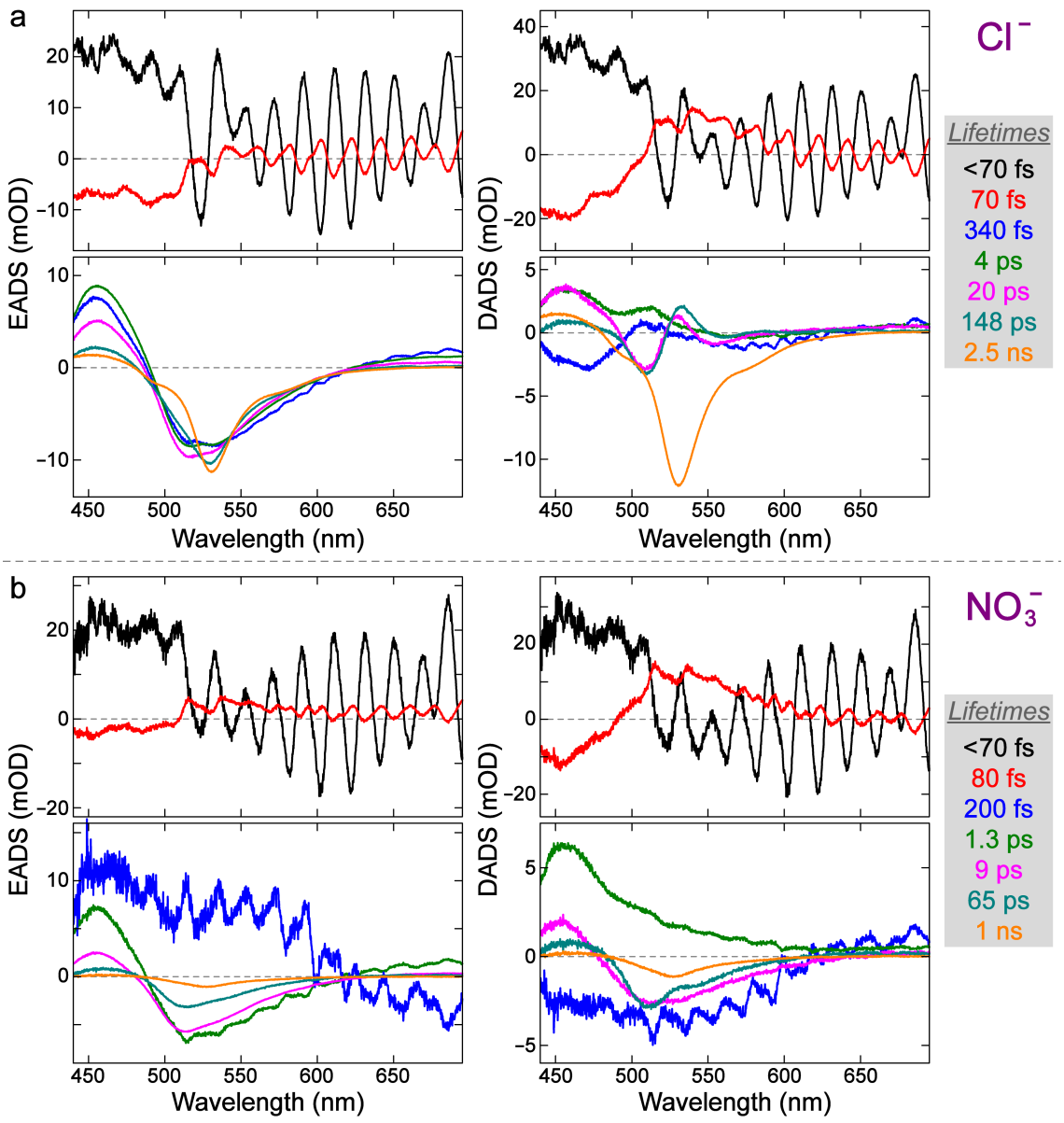

Figure S6. Global analysis for fs-TA spectra of phiYFP with 400 mM (a) Cl^- and (b) NO_3^- in 50 mM MES buffer at pH=5.5. The evolution-associated difference spectra (EADS, left panels) and decay-associated difference spectra (DADS, right panels) can be compared with the species-associated difference spectra (SADS, see **Fig. 5** in main text). The lifetimes are provided with the same colors as the corresponding spectral components retrieved from the least-squares fits. The first two components (black and red) are separated from the rest of EADS/DADS to avoid congestion for better presentation of all the spectral traces across the sub-ps to ns timescales.

Notably, the spectral chirp in these ultrafast coherent spectroscopic data has been largely corrected by the chirped mirror pairs in our optical setup,[2] and the SADS (see **Fig. 5** in main text) are chirp-corrected spectra (further minimized by a mathematical approach using Glotaran software[5]) during global analysis. The probe wavelength region above ~520 nm is affected by coherent artefacts near the photoexcitation time zero (**Fig. 5** top panels). However, the probe region below ~520 nm, though convolved with some coherent artefacts, exhibits clear positive and negative bands with distinct profiles and magnitudes in the early-time FC and A* (**Fig. 5** top panels) as black and red traces, respectively, and therefore cannot be ascribed to artefacts only. In fact, the systematic and comparative global analysis for wild-type phiYFP in the presence of 400 mM Cl^- and NO_3^- substantiates the validity of A* SADS with a characteristic stimulated emission (SE) band below 500 nm, in good agreement with their steady-state emission wavelength at ~460–470 nm (see **Fig. 2**, **Fig. S2**, and **Table 1**).

Furthermore, the DADS (see **Fig. S6a**, lower right panel) and SADS (**Fig. 5b**, middle panel) of the TICT component (colored in blue) show red-shifted SE bands from the fluorescence peak (clear for phiYFP with Cl^-, albeit a bit less clear for phiYFP with NO_3^-), while the DADS/SADS of the HGS component (colored in green) exhibit nearly identical positive absorption features. Such distinct spectral features clearly distinguish these two underlying components from the rest of transient states/species, i.e., A*, I_1*, and I_2* that are characterized by prominent SE bands at ~460–470, 510, and 530 nm, respectively (e.g., see **Fig. 5b,c** middle and bottom panels). Therefore, the presence of TICT state is validated by interwoven experimental observations and analysis results in this work, which is also corroborated by various published theoretical works on GFP ultrafast energy dissipation and isomerization pathways from gas phase[16-19] to solution phase.[8,20]

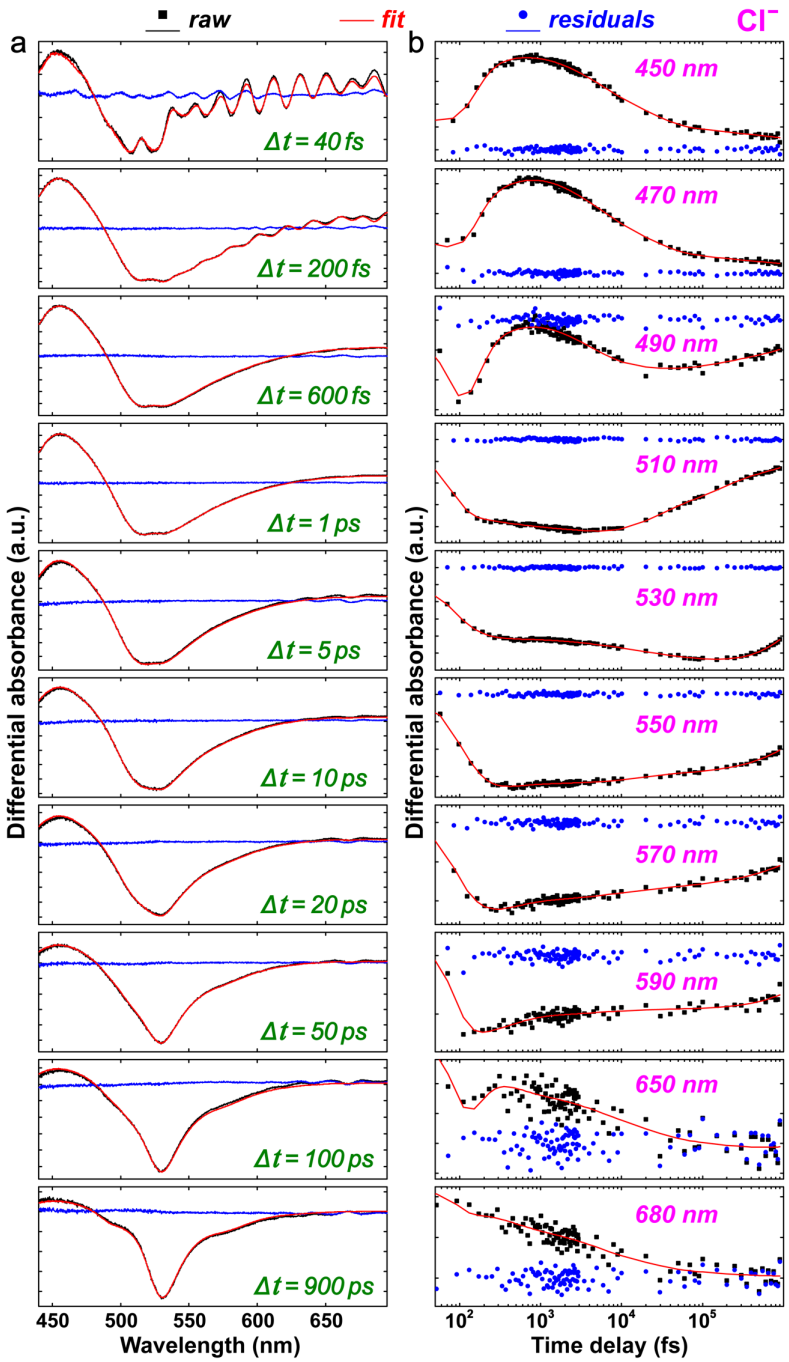

Figure S7. Fit quality and residuals of target analysis for phiYFP with 400 mM Cl^- in 50 mM MES buffer at pH=5.5. Raw fs-TA spectra (black) (a) at representative time delay points (green) across our detection window of 900 ps and (b) at representative probe wavelengths (magenta) across a spectral region over 250 nm are overlaid with least-squares fits (red) from global analysis, and the residuals around zero optical density (OD) are shown in blue.

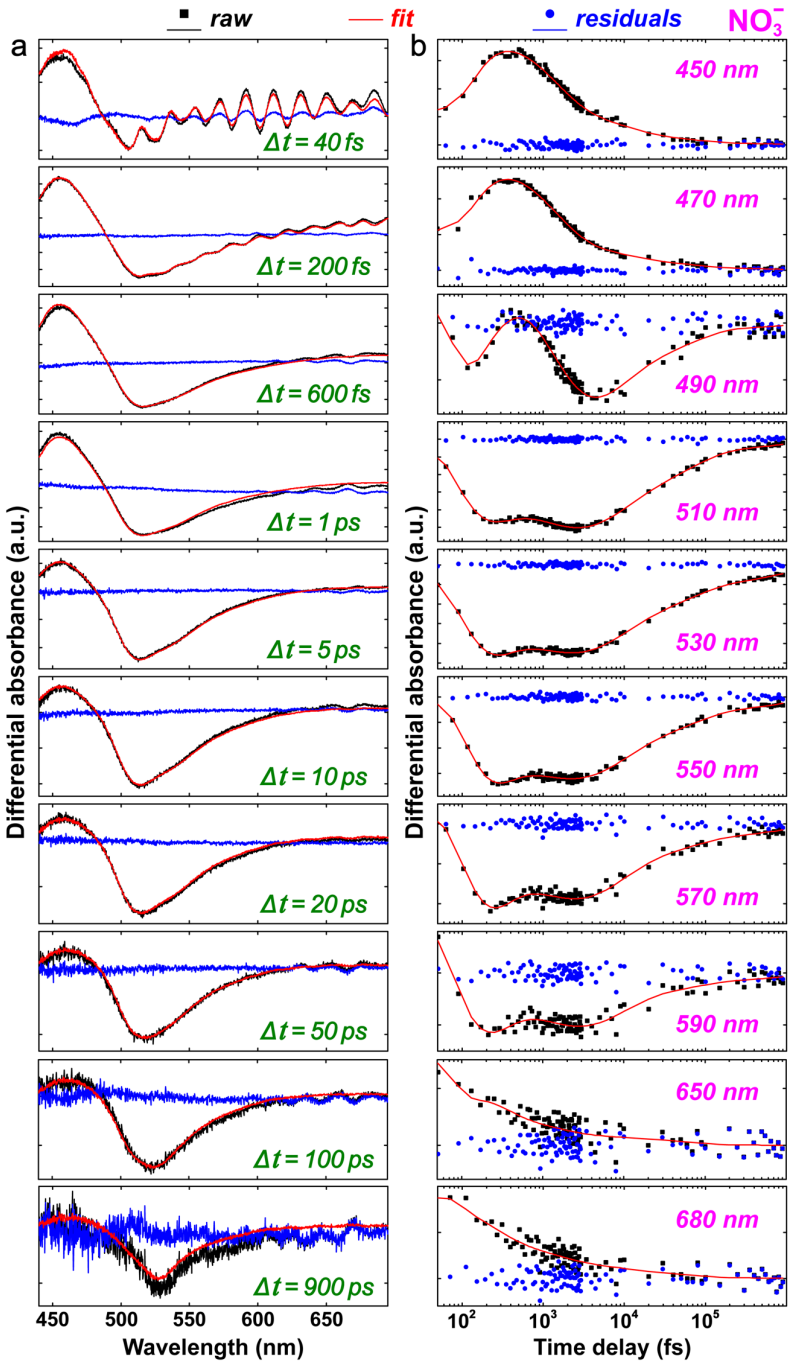

Figure S8. Fit quality and residuals of target analysis for phiYFP with 400 mM NO_3^- in 50 mM MES buffer at pH=5.5. Raw fs-TA spectra (black) (a) at representative time delay points (green) across our detection window of 900 ps and (b) at representative probe wavelengths (magenta) across a spectral region over 250 nm are overlaid with least-squares fits (red) from global analysis, and the residuals around zero OD are shown in blue.

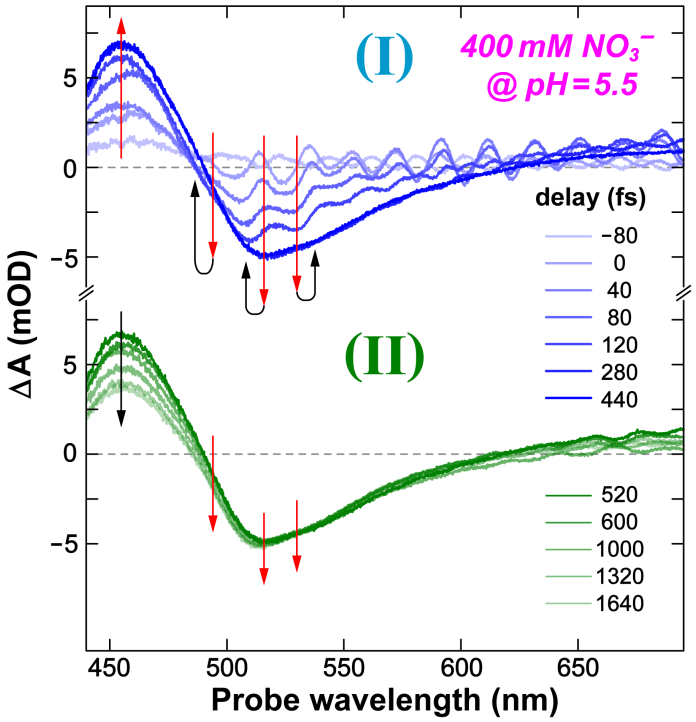

Figure S9. Stages I and II of the fs-TA spectra for phiYFP with 400 mM NO_3^- in 50 mM MES buffer at pH=5.5. Red and black arrows denote the transient electronic peak intensity magnitude rise and decay, respectively. The subsequent stages III and IV are displayed in **Figure 3c** (main text), while the probe-dependent kinetic plots at key ESA and SE bands are presented in **Figure 4b** (highlighting the ultrafast rise-decay-rise pattern at 510 and 530 nm within the prominent broad SE band, in accord with the red→curved-black→red arrows before ~2 ps in this figure).

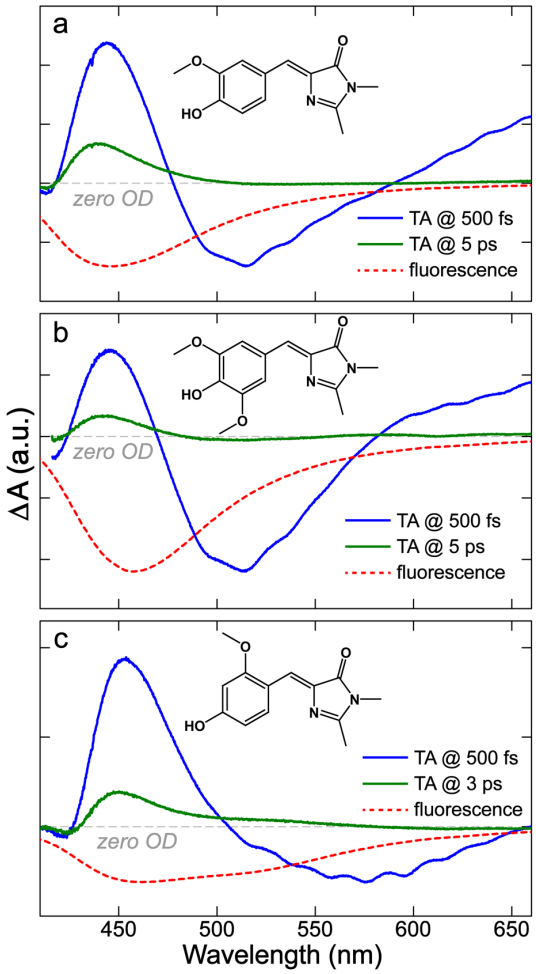

Figure S10. Typical fs-TA spectra of nonfluorescent neutral avGFP chromophore analogues. The excitation wavelength was provided at 400 nm. Methanol was used as the solvent to suppress excited-state proton transfer and focus on the light-induced chromophore twisting motions.[3] These newly synthesized GFP chromophore derivatives[21] will be reported in a future publication.

For GFP chromophore and its structural analogues (e.g., methoxy-HBDIs) bearing a flexible methine bridge (R_1−CH=R_2),[8,22] the TA spectra usually feature a twisted intramolecular charge transfer (TICT) state that is characterized by a red-shifted SE band with respect to the fluorescence band as well as a blue ESA band.[8] The SE band at the fluorescent peak is often not observed due to the ultrashort lifetime of the neutral chromophore and spectral overlap with ESA bands. The TICT state is often accompanied by a vibrationally unrelaxed "hot" ground state as observed.[8,23]

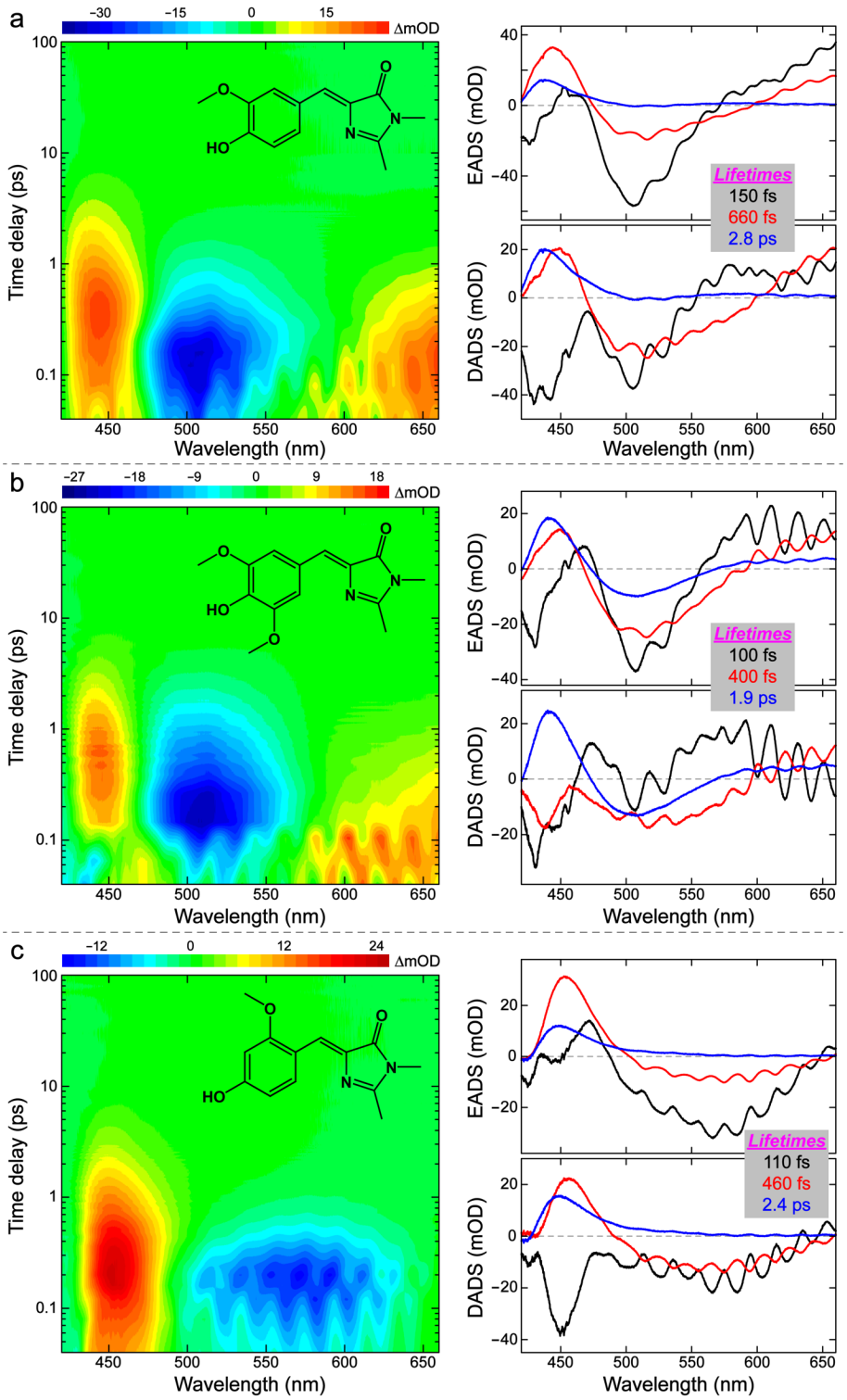

Figure S11. Contour plots (left) and global analysis (right) of the fs-TA spectra of three GFP chromophore analogues in methanol after 400 nm excitation. Color-coded lifetimes of the retrieved components are listed. The selected spectra in **Figure S10** are taken from the fs-TA data herein.

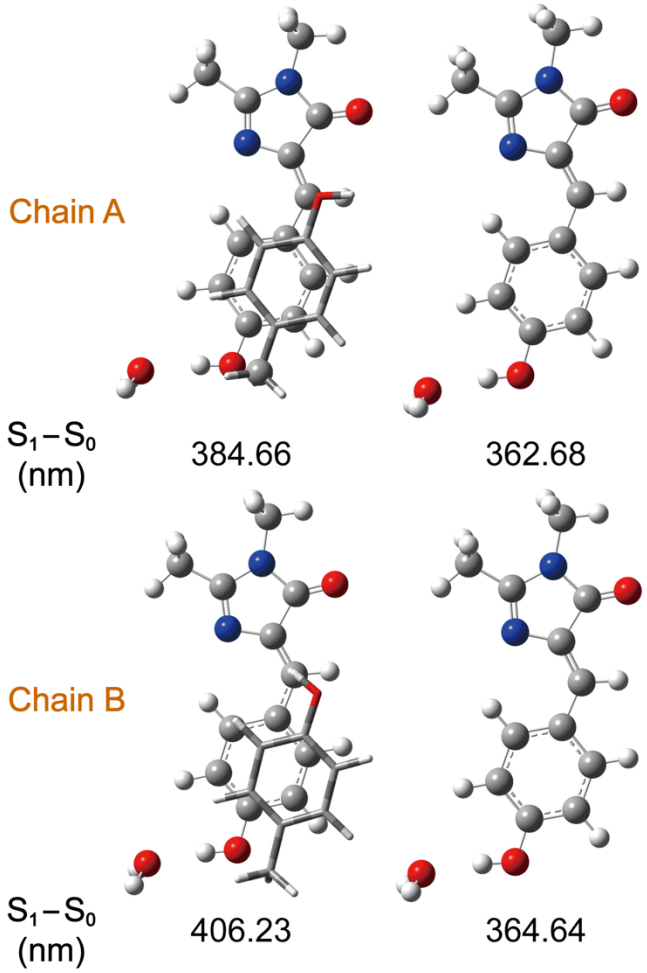

Figure S12. Calculated absorption gap of the neutral chromophore for phiYFP. The two chains of the crystal structure of phiYFPv (PDB ID: 4HE4)[9] are shown in the upper (Chain A) and lower (Chain B) panels. The antiparallel π-π stacking of the chromophore Y66 and the proximal Y203 (left panels) exhibit a notable redshift of the S_0–S_1 energy gap (in nanometer/nm unit) *versus* the isolated chromophore (right panels). A conserved water molecule near the chromophore Y66 phenolic hydroxyl was included in the calculation (see Section 1.4 above for details). Note that phiYFPv differs from its progenitor wild-type phiYFP by ten amino-acid residues that are outside the chromophore area and mostly positioned on the protein surface exposed to solvent, therefore it is still a good representation of the chromophore immediate environment and spectral properties.

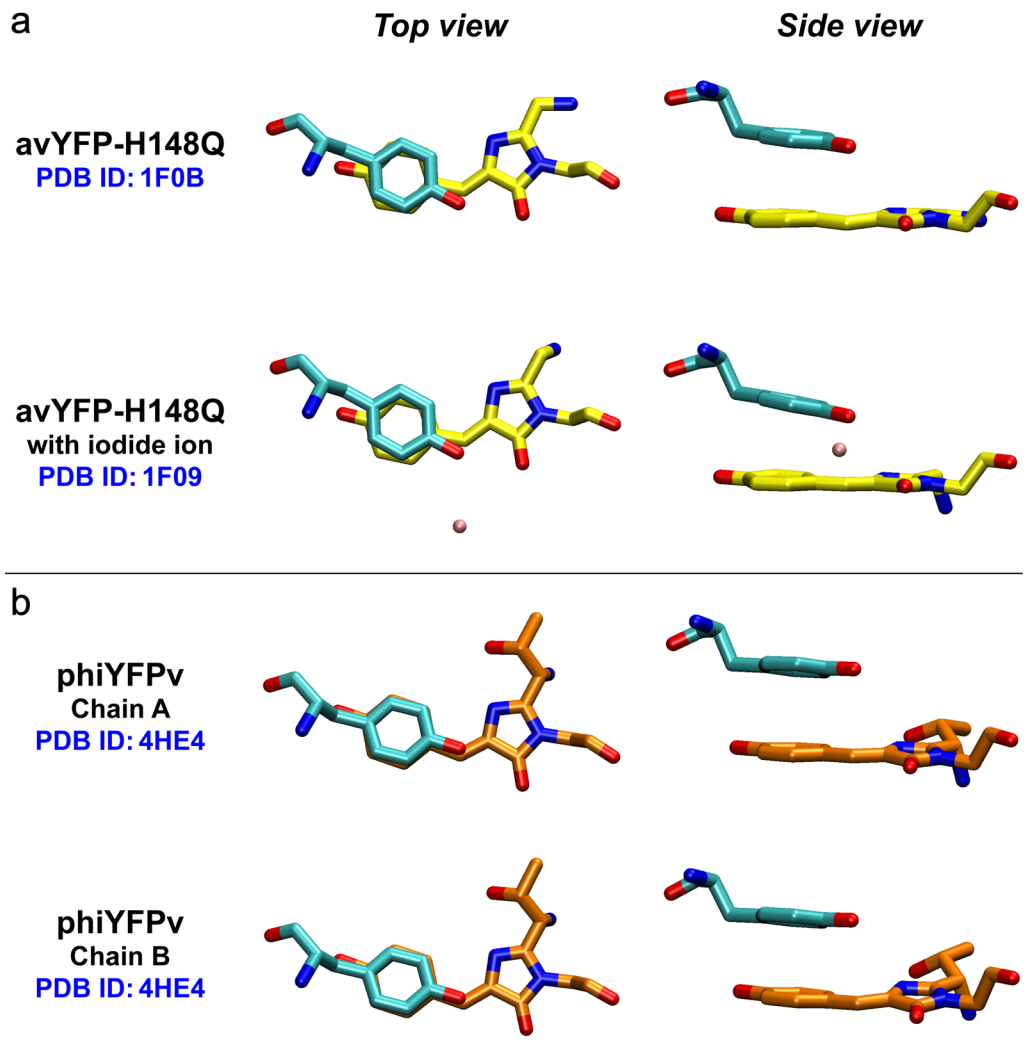

Figure S13. Perspectives of π-π stacking in avYFP-H148Q and phiYFPv crystal structures. The chromophore of avYFP-H148Q in (a) is mainly in the neutral form[10] while that of phiYFPv in (b) is in the anionic form.[9] Y203 is shown in cyan, and the bound iodide is shown as a pink sphere.

For avYFP-H148Q, the iodide binding causes deviations from the antiparallel conformation in terms of π-π stacking between the chromophore Y66 and Y203 mainly due to the electrostatic interaction between the iodide and Y203 hydroxyl (see **Figure S13a** lower panels, top and side views), which accounts for the blueshift of the neutral chromophore absorption peak *versus* that in phiYFPv with better π-π stacking (**Figure S13b**). This likely explains a redder emission from the deprotonated chromophore inside phiYFP than avYFP-H148Q (i.e., 542 > 529 nm, see **Table 1**).

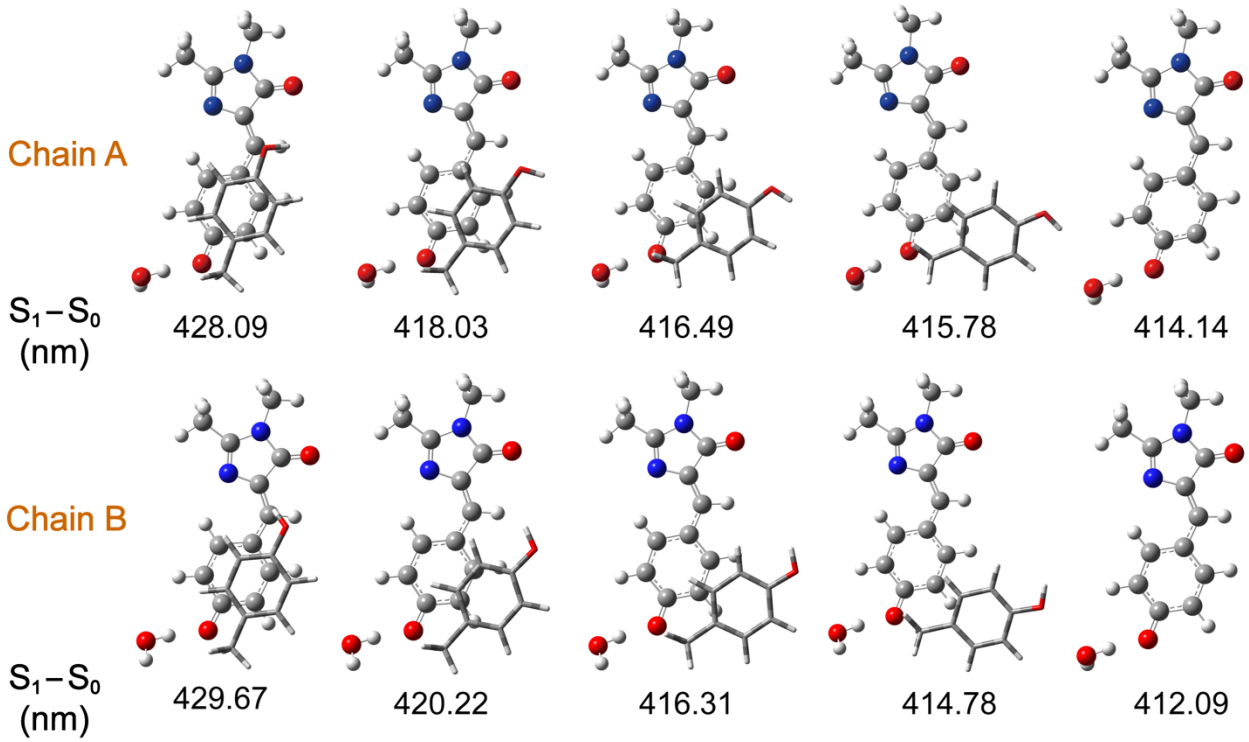

Figure S14. Calculated S_0–S_1 energy gap of the anionic chromophore in phiYFPv. Two chains of phiYFPv are listed in the upper (Chain A) and lower (Chain B) panels in the order from left to right: π-π stacked (taken from PDB ID: 4HE4),[9] Y203 side-chain phenol ring shifted away from the antiparallel configuration by 20°, 40°, and 60°, and no Y203 side chain. The $S_0 \rightarrow S_1$ vertical transition energy gap (absorption) in nanometer (nm) unit is labeled below each structure.

Notably, for the deprotonated chromophore, rotating the Y203 side chain away to disrupt π-π stacking induces a clear blueshift of the electronic transition (we focus on the trend, not absolute values due to limitations in our DFT calculations).[3] This is consistent with our hypothesis that a slightly larger, trigonal NO_3^- group with stronger binding affinity would distort the binding site, causing Y203 to be in a less conjugated position with the chromophore (e.g., **Figure S13a**) and thus hindering $I_1^* \rightarrow I_2^*$ conversion, than the relatively more flexible Y203 in the spherical-Cl^--bound phiYFP that can better π-π stack with the chromophore Y66 phenolate (**Figures 6** and **S1**).

3. Supplementary Tables

Table S1. Absorption and emission peak wavelengths of phiYFP at pH=5.5 and 4.5

		Absorption (nm)		Emission (nm)[b]			
		A	B	A*	I_1*	I_2*	B*
pH=5.5[a]	Cl^-	403	526	470	504	542	542
	NO_3^-	402	524	463	506	534	534
pH=4.5[a]	Cl^-	403	–[c]	462	507	–[d]	530
	NO_3^-	403	–[c]	462	506	–[d]	520

[a] For pH=5.5 and 4.5 aqueous solution, 50 mM MES buffer and 50 mM sodium citrate buffer were used, respectively, with 400 mM Cl^- or NO_3^- (see Experimental Section 1.1 above). The phiYFP spectral data in pH=5.5 buffer solution are identical to those listed in **Table 1** (main text).

[b] The emission wavelengths were obtained from the 2nd derivative analysis (**Figures S2** and **S4**).

[c] Difficult to determine due to the very low population at this pH condition.

[d] Not present because the chromophore is trapped in the I_1* state at this pH condition.

Table S2. Probe-wavelength-dependent dynamics in fs-TA for phiYFP at pH=5.5[a]

	wavelength/nm	τ_1/fs[b]	τ_2/fs[b]	τ_3/fs[b]	τ_4/ps[b]	τ_5/ps[b]	τ_6/ps[b]	τ_7/ns[b]
Cl^-	450	180 (+)	n.a.	n.a.	5.6 (−)	43 (−)	n.a.	1.8 (−)
	500	90 (+)	110 (−)	540 (+)	8.6 (+)	14 (−)	122 (−)	2.2 (−)
	510	<70 (+)	n.a.	550 (+)	2.1 (+)	31 (−)	132 (−)	2.1 (−)
	530	70 (+)	n.a.	540 (+)	2.2 (+)	36 (+)	406 (+)	1.9 (−)
NO_3^-	450	350 (+)	n.a.	690 (−)	2.5 (−)	15 (−)	100 (−)	n.a.
	500	100 (+)	170 (−)	980 (+)	n.a.	14 (−)	76 (−)	1.0 (−)
	510	<70 (+)	360 (−)	740 (+)	n.a.	14 (−)	73 (−)	0.7 (−)
	530	90 (+)	270 (−)	790 (+)	2.2 (+)	12 (−)	71 (−)	1.3 (−)

[a] The aqueous solution consists of 50 mM MES buffer with 400 mM Cl^- or NO_3^-.

[b] The "+" and "−" denote the rise and decay components from least-squares fits, respectively. "n.a." stands for not applicable. In the "Cl^-" rows, the complementary time constants retrieved from fs-TA dynamics are highlighted by the orange shades. The slight mismatch between time constants for each process may arise from the TA spectral overlap (see main text).[3,6,15] The corresponding least-squares fits of spectral data points for top two rows and bottom two rows of Cl^-/NO_3^- samples can be found in **Figure S5a/b** and **Figure 4a/b**, respectively.

4. Supplementary References

(1) Tutol, J. N.; Peng, W.; Dodani, S. C. Discovery and Characterization of a Naturally Occurring, Turn-On Yellow Fluorescent Protein Sensor for Chloride. *Biochemistry* **2019**, *58*, 31-35.

(2) Tang, L.; Zhu, L.; Taylor, M. A.; Wang, Y.; Remington, S. J.; Fang, C. Excited State Structural Evolution of a GFP Single-Site Mutant Tracked by Tunable Femtosecond-Stimulated Raman Spectroscopy. *Molecules* **2018**, *23*, 2226.

(3) Fang, C.; Tang, L.; Chen, C. Unveiling Coupled Electronic and Vibrational Motions of Chromophores in Condensed Phases. *J. Chem. Phys.* **2019**, *151*, 200901.

(4) Liu, W.; Han, F.; Smith, C.; Fang, C. Ultrafast Conformational Dynamics of Pyranine during Excited State Proton Transfer in Aqueous Solution Revealed by Femtosecond Stimulated Raman Spectroscopy. *J. Phys. Chem. B* **2012**, *116*, 10535-10550.

(5) Snellenburg, J. J.; Laptenok, S. P.; Seger, R.; Mullen, K. M.; van Stokkum, I. H. M. Glotaran: A Java-Based Graphical User Interface for the R-Package TIMP. *J. Stat. Softw.* **2012**, *49*, 1-22.

(6) van Stokkum, I. H. M.; Larsen, D. S.; van Grondelle, R. Global and Target Analysis of Time-Resolved Spectra. *Biochim. Biophys. Acta* **2004**, *1657*, 82-104.

(7) Chen, C.; Liu, W.; Baranov, M. S.; Baleeva, N. S.; Yampolsky, I. V.; Zhu, L.; Wang, Y.; Shamir, A.; Solntsev, K. M.; Fang, C. Unveiling Structural Motions of a Highly Fluorescent Superphotoacid by Locking and Fluorinating the GFP Chromophore in Solution. *J. Phys. Chem. Lett.* **2017**, *8*, 5921–5928.

(8) Taylor, M. A.; Zhu, L.; Rozanov, N. D.; Stout, K. T.; Chen, C.; Fang, C. Delayed Vibrational Modulation of the Solvated GFP Chromophore into a Conical Intersection. *Phys. Chem. Chem. Phys.* **2019**, *21*, 9728-9739.

(9) Pletneva, N. V.; Pletnev, V. Z.; Souslova, E.; Chudakov, D. M.; Lukyanov, S.; Martynov, V. I.; Arhipova, S.; Artemyev, I.; Wlodawer, A.; Dauter, Z.; et al. Yellow Fluorescent Protein phiYFPv (*Phialidium*): Structure and Structure-Based Mutagenesis. *Acta Crystallogr. D* **2013**, *69*, 1005-1012.

(10) Wachter, R. M.; Yarbrough, D.; Kallio, K.; Remington, S. J. Crystallographic and Energetic Analysis of Binding of Selected Anions to the Yellow Variants of Green Fluorescent Protein. *J. Mol. Biol.* **2000**, *301*, 157-171.

(11) Arosio, D.; Garau, G.; Ricci, F.; Marchetti, L.; Bizzarri, R.; Nifosì, R.; Beltram, F. Spectroscopic and Structural Study of Proton and Halide Ion Cooperative Binding to GFP. *Biophys. J.* **2007**, *93*, 232-244.

(12) Frisch, M. J.; Trucks, G. W.; Schlegel, H. B.; Scuseria, G. E.; Robb, M. A.; Cheeseman, J. R.; Scalmani, G.; Barone, V.; Petersson, G. A.; Nakatsuji, H.; et al. *Gaussian 16, Revision A.03*; Gaussian, Inc.: Wallingford, CT, 2016.

(13) Chattoraj, M.; King, B. A.; Bublitz, G. U.; Boxer, S. G. Ultra-Fast Excited State Dynamics in Green Fluorescent Protein: Multiple States and Proton Transfer. *Proc. Natl. Acad. Sci. U. S. A.* **1996**, *93*, 8362-8367.

(14) Oscar, B. G.; Liu, W.; Zhao, Y.; Tang, L.; Wang, Y.; Campbell, R. E.; Fang, C. Excited-State Structural Dynamics of a Dual-Emission Calmodulin-Green Fluorescent Protein Sensor for Calcium Ion Imaging. *Proc. Natl. Acad. Sci. U. S. A.* **2014**, *111*, 10191-10196.

(15) Fang, C.; Tang, L. Mapping Structural Dynamics of Proteins with Femtosecond Stimulated Raman Spectroscopy. *Annu. Rev. Phys. Chem.* **2020**, *71*, 239-265.

(16) Martin, M. E.; Negri, F.; Olivucci, M. Origin, Nature, and Fate of the Fluorescent State of the Green Fluorescent Protein Chromophore at the CASPT2//CASSCF Resolution. *J. Am. Chem. Soc.* **2004**, *126*, 5452-5464.

(17) Olsen, S.; Smith, S. C. Bond Selection in the Photoisomerization Reaction of Anionic Green Fluorescent Protein and Kindling Fluorescent Protein Chromophore Models. *J. Am. Chem. Soc.* **2008**, *130*, 8677-8689.

(18) Polyakov, I. V.; Grigorenko, B. L.; Epifanovsky, E. M.; Krylov, A. I.; Nemukhin, A. V. Potential Energy Landscape of the Electronic States of the GFP Chromophore in Different Protonation Forms: Electronic Transition Energies and Conical Intersections. *J. Chem. Theory Comput.* **2010**, *6*, 2377-2387.

(19) Svendsen, A.; Kiefer, H. V.; Pedersen, H. B.; Bochenkova, A. V.; Andersen, L. H. Origin of the Intrinsic Fluorescence of the Green Fluorescent Protein. *J. Am. Chem. Soc.* **2017**, *139*, 8766-8771.

(20) Altoe, P.; Bernardi, F.; Garavelli, M.; Orlandi, G.; Negri, F. Solvent Effects on the Vibrational Activity and Photodynamics of the Green Fluorescent Protein Chromophore: A Quantum-Chemical Study. *J. Am. Chem. Soc.* **2005**, *127*, 3952-3963.

(21) Chen, C.; Fang, C. Devising Efficient Red-Shifting Strategies for Bioimaging: A Generalizable Donor-Acceptor Fluorophore Prototype. *Chem. Asian J.* **2020**, *15*, 1514-1523.

(22) Mandal, D.; Tahara, T.; Meech, S. R. Excited-State Dynamics in the Green Fluorescent Protein Chromophore. *J. Phys. Chem. B* **2004**, *108*, 1102-1108.

(23) Tang, L.; Fang, C. Nitration of Tyrosine Channels Photoenergy through a Conical Intersection in Water. *J. Phys. Chem. B* **2019**, *123*, 4915-4928.